Increasing Eukaryotic Initiation Factor 6 (eIF6) Gene Dosage Stimulates Global Translation and Induces a Transcriptional and Metabolic Rewiring that Blocks Programmed Cell Death

Arianna Russo[1,2], Guido Gatti[1,3], Roberta Alfieri[1], Elisa Pesce[1], Kelly Soanes[4], Sara Ricciardi[1,3], Cristina Cheroni[1], Thomas Vaccari[3], Stefano Biffo[1,3]*, Piera Calamita[1,3]*

[1] INGM, National Institute of Molecular Genetics, "Romeo ed Enrica Invernizzi", Milan, Italy

[2] DiSIT, University of Eastern Piedmont, Alessandria, Italy

[3] DBS, Università degli Studi di Milano

[4] Aquatic and Crop Resource Development - National Research Council of Canada

*These authors contributed equally to this work

Address correspondence to Piera Calamita or Stefano Biffo Via Francesco Sforza 35 20122 Milano Italia. calamita@ingm.org; biffo@ingm.org

Short Title: DeIF6 regulates translation, PCD and 20-HE signaling

ABSTRACT

Increases in ribosomal proteins and initiation factors are often observed in tumours and required during development. Haploinsufficient models have shown that such elevation is essential for tumour growth. Models with increased gene dosage of initiation factors, addressing the effects of their forced overexpression are lacking. The eukaryotic Initiation Factor 6 (eIF6) gene is amplified in some cancers and overexpressed in most, while it has been demonstrated that eIF6 haploinsufficiency protects mice from lymphomagenesis. eIF6 is necessary for ribosome biogenesis and efficient translation, and is present as a single gene in all animal species. Taking advantage of genetic tractability of *Drosophila melanogaster*, we generated an *in vivo* model of eIF6 upregulation, in order to assess the early effects of increased gene dosage of this initiation factor. eIF6 overexpression increases the general rate of translation, both *in vivo* and *in vitro*. Organ specific overexpression in the eye causes a rough phenotype. The increase of translation driven by eIF6 is accompanied by a complex transcriptional rewiring and a modulation of histone acetylation activity. Gene expression changes caused by eIF6 include a dominant upregulation of ribosome biogenesis, a shift in Programmed Cell Death (PCD) and inhibition of ecdysteroids biosynthesis. Administration of 20-HydroxyEcdysone or expression of p35 apoptotic modulator reverts some of the effects driven by high eIF6 levels. We conclude that the increased translation driven by high levels of eIF6 generates a transcriptional and hormonal rewiring that evidences the capability of the translational machinery to regulate specific gene expression and metabolism. In addition, our *in vivo* model could be useful to screen potential drugs to treat cells with altered *eIF6* gene dosage.

AUTHOR SUMMARY

The eukaryotic Initiation Factor eIF6 is necessary for ribosome biogenesis and translation initiation and is upregulated or amplified at genetic level in some cancers. Mice haploinsufficient for eIF6 are protected from lymphomagenesis, but a model with increased gene dosage of this initiation factor was still lacking. We present here a thorough analysis on the early effects due to amplified *DeIF6* in *Drosophila melanogaster*. We show that an increase of *DeIF6* gene dosage results in an increase of general translation able to modulate transcription of genes involved in ribosome biogenesis, programmed cell death and ecdysone biosynthesis.

57 **INTRODUCTION**

58 Ribosomal Proteins (RPs) and eukaryotic Initiation Factors (eIFs) are necessary for
59 two major cellular processes: ribosome biogenesis and translation (1-5). It has been
60 now widely established that downregulation of RPs and eIFs can protect from cancer
61 (6).

62 Proteins involved in ribosome biogenesis do not usually have a role in the
63 translational control and *vice versa* (7). However, the eukaryotic Initiation Factor 6
64 (eIF6) is remarkably unique (8): around 20% is essential for nucleolar maturation of
65 the 60S large subunit of the ribosome (9), while cytoplasmic eIF6 acts as a
66 translation factor necessary for fatty acid synthesis and glycolysis through translation
67 of transcription factors such as CEBP/β, ATF4 and CEBP/δ containing G/C rich or
68 uORF sequences (10, 11). Mechanistically, eIF6 is an anti-association factor: by
69 binding to the 60S subunit, it prevents its premature joining with a 40S not loaded
70 with the preinititiaton complex. Release of eIF6 is then mandatory for the formation
71 of an active 80S (12).

72 eIF6 is highly conserved in yeast, *Drosophila* and humans (13). During evolution, the
73 *eIF6* gene has not been subjected to gene duplication. Despite ubiquitous
74 expression, eIF6 levels *in vivo* are tightly regulated in physiological conditions,
75 showing considerable variability of expression among different tissues (14).
76 Importantly, high levels of eIF6 or hyperphosphorylated eIF6 are observed in some
77 cancers (15, 16), and are rate limiting for tumour onset and progression in mice (17).
78 In addition, eIF6 amplification is observed in luminal breast cancer patients (18) and
79 may affect also migration (19). However, whether eIF6 overexpression *per se* can
80 change a transcriptional program in the absence of other genetic lesions is unknown.

81 Taking advantage of the high sequence similarity among *eIF6* homologues, here we
82 used *Drosophila melanogaster*, an ideal model to manipulate gene expression in a
83 time- and tissue-dependent manner, using the GAL4/UAS system (19, 20) to study
84 the effects of *eIF6* increased gene dosage *in vivo*. Such a gain of function approach
85 allowed us to investigate which are the effects of eIF6 overexpression in the context
86 of an intact organ. We used the fly eye, an organ not essential for viability, whose
87 development from epithelial primordia, the larval eye imaginal disc, is well
88 understood. The adult fly compound eye is a stunningly beautiful structure of
89 approximately 800 identical units, called ommatidia (21). Each ommatidium is
90 composed of eight neuronal photoreceptors, four glial-like cone cells and pigment
91 cells (22, 23). By increasing DeIF6 levels in the eye, we have found alterations in
92 physiological apoptosis at the pupal stage, correlating with an increase in general
93 translation. Importantly, we also observed a reshaping of the eye transcriptome that
94 revealed a coordinated downregulation of the ecdysone biosynthesis pathway.
95 Overall, our study provides the first *in vivo* evidence of an increase in translation
96 dependent on a heightened *eIF6* gene dosage, which drives metabolic changes and
97 a transcriptional rewiring of a developing organ. Our model provides a new and
98 simple way to screen for therapeutic molecules relevant for cancers with aberrant
99 *eIF6* gene dosage and suggest that overexpression of a translation factor *per se*
100 may induce a new gene expression program.
101

102 **RESULTS**

103 **Alterations of DeIF6 levels results in early embryonic lethality and aberrant**
104 **organ morphology**

105 We first assessed the effects caused by the loss of the *Drosophila* homologue of
106 *eIF6*, *DeIF6*. To this end, we used the *P* element allele $eIF6^{k13214}$ (24), inducing
107 mitotic clones homozygous for $eIF6^{k13214}$ in first instar larvae by heat shock-induced
108 FLIP/*FLP*-mediated homologous recombination (25). We did not observe clones of
109 eIF6 mutant cells with the exception of small ones in the wing margin. Similar results
110 were obtained in a *minute* (M) background that provides a growth advantage to
111 mutant cells, or by targeted expression of FLP in the wing margin (S1A Fig).
112 Together, these results indicate that eIF6 is required for cell viability in *Drosophila*,
113 as previously observed in yeast (16) and mammals (9) and preclude significant
114 studies on the value of its inhibition, a phenomenon absent in physiological
115 conditions.

116 To assess the effects of the gain of function, which is often observed *in vivo* in
117 cancer, we overexpressed *DeIF6* ubiquitously using the *TubGAL4* driver. Ectopic
118 expression resulted in late embryonic lethality (S1B Fig), suggesting that increased
119 levels of eIF6 disrupt gene expression. To circumvent early lethality, we focused on
120 a non-essential fly organ, the eye. DeIF6 overexpression during late larval eye disc
121 development, by the *GMRGAL4* driver (*GMR>DeIF6*), caused the formation of a
122 rough adult eye (Fig 1A-B). Eye roughness is often observed in mutants that alter the
123 fine structure of the compound eye (26-29). Indeed, SEM analysis showed severe
124 disruption of the stereotypic structure of the wild-type eye, with flattened ommatidia
125 and bristles arranged in random patterns (Fig 1C). Semithin sections evidenced that
126 the roughness was due to an aberrant arrangement and morphology of cells (Fig 1D).

127 These data show that elevated *DeIF6* gene dosage in the *Drosophila* eye causes a
128 strong phenotype, that we further chatacterized.
129
130 **Increased *DeIF6* gene dosage results in elevated translation**
131 eIF6 binds free 60S *in vitro* and *in vivo* affecting translation (8). In order to assess
132 the effects of overexpressed DeIF6 *in vivo* on the translational machinery, we first
133 investigated whether it led to a change in free 60S subunits, *in vivo*. To this end, we
134 used a recently developed assay, the *in vitro* Ribosome Interaction Assay (iRIA) (30).
135 We found that the expression of DeIF6 in larval eye discs (*GMR>DeIF6*) led to 25%
136 reduction of free 60S sites when compared to control (*GMRGAL4/+*) (Fig 1E). Next,
137 using a modified SUnSET assay (31), we measured translation in eye imaginal discs
138 treated *ex vivo* with puromycin, incorporated in protein nascent chains by ribosomes.
139 Remarkably, *GMR>DeIF6* eye discs incorporated almost twice the amount of
140 puromycin of controls (Fig 1F-G). Taken together, high levels of eIF6 increase the
141 free 60S pool *in vivo*, and increase puromycin incorporation, i.e. translation.
142 To evaluate whether increased puromycin incorporation upon eIF6 overexpression
143 was specific to *Drosophila*, we overexpressed human eIF6 in HEK293T cells, grown
144 upon serum stimulation, and examined puromycin incorporation with a
145 cytofluorimeter. Upon eIF6 2-fold expression relative to control (S1C Fig), we
146 observed an increase in puromycin incorporating cells (S1D-E Fig). These data
147 demonstrate that increased eIF6 leads, in the presence of appropriate extracellular
148 signals or growth factors, to an elevation of the general translational rate, both *in vivo*
149 and *in vitro*.
150
151 **Increased *DeIF6* gene dosage alters physiological apoptosis**

152 To understand how deregulated protein synthesis leads to the tissue defects
153 observed upon DeIF6 overexpression, we first performed a thorough analysis of eye
154 development. Larval eye discs revealed no differences in morphology or cell identity
155 compared to controls (S2A-C Fig). Then, we analyzed the effect of *DeIF6* increased
156 gene dosage during pupal development. We found that at 40h after puparium
157 formation (APF) both neuronal and cone cells were present in the correct number.
158 Conversely, we observed that the ommatidial morphology was altered (Fig 2). One of
159 the fundamental events controlling ommatidial morphology is a developmentally-
160 controlled wave of PCD, sweeping the tissue from 25h to 42h APF (23). At 28h APF,
161 TUNEL assay showed the absence of apoptotic nuclei in the *GMR>DeIF6* retinae,
162 whereas *GMRGAL4/+* retinae showed many of them (S3A Fig). Next, we analyzed
163 the *Drosophila* effector caspase Dcp-1 by immunostaining at 40h APF. Compared to
164 control retinae showing the presence of apoptotic cells, these were completely
165 absent in *GMR>DeIF6* retinae (Fig 3A). Next, 60h APF *GMR>DeIF6* retinae showed
166 Dcp-1 positive cells. In contrast, 60h APF wild-type retinae did not show any
167 apoptotic cell, confirming that developmental PCD had correctly ended by then (Fig
168 3B). We determined the number of Dcp-1 positive cells at 40h APF and 60h APF
169 (Fig 3C), revealing a striking 75% reduction in the number of apoptotic cells at 40h
170 APF in *GMR>DeIF6*, and an 80% increase at 60 hours APF. A change in apoptosis
171 dynamics was confirmed by staining for the *Drosophila* β-catenin homologue
172 Armadillo (Fig 4). Armadillo localizes to membranes of cells surrounding
173 photoreceptors, providing an indication of their number. At 40h APF, we observed
174 that control retinae presented the typical staining expected for Armadillo, while
175 *GMR>DeIF6* retinae showed the presence of extra-numerary cells around the
176 ommatidial core (Fig 4A), in line with the possibility that these were not removed by

177 PCD. By counting the number of cells in each ommatidium, we determined that
178 *GMR>DeIF6* retinae possessed more than 15 cells, corresponding to approximately
179 30% more than that of a wild-type ommatidium (S4A Fig). Later in development, both
180 at 60h and 72h APF, while in wild-type retinae the pattern of Armadillo was
181 maintained, in *GMR>DeIF6* retinae Armadillo was no longer detectable (Fig 4B and
182 S4B Fig), indicating the late PCD inappropriately removes most inter-ommatidial
183 cells (IOCs). In conclusion, the early effect of eIF6 high levels is a block of apoptosis
184 that may then in turn lead to a disrupted developmental program.
185

186 **Restricting the increase of *DeIF6* gene dosage to cone and IOCs is sufficient to**
187 **alter PCD**

188 Both cone and inter-ommatidial cells (IOCs) signal for the correct removal of extra-
189 numerary cells by PCD to determine the correct number of ommatidial cells (32).
190 Thus, to determine which cell type is responsible for the altered PCD, we increased
191 DeIF6 levels in either one of these two cell types, with the *spaGAL4* or *54CGAL4*
192 drivers, respectively. Here, the increased expression of DeIF6 resulted in a rough
193 eye phenotype, albeit a milder one with respect to the one observed with the
194 *GMRGAL4* driver (Fig 5A, S5A Fig). Semithin sections of *spa>DeIF6* adult eyes
195 confirmed the loss of the eye structure and, similarly to *GMR>DeIF6*, revealed that
196 cellular arrangement and morphology were altered (Fig 5B). Characterization of
197 pupal *spa>DeIF6* retinae confirmed that DeIF6 expression was confined to cone
198 cells (Fig 5C). In addition, similar to *GMR>DeIF6* retinae, the staining of the markers
199 ELAV and CUT demonstrated that cell identity was maintained, but that arrangement
200 of cells on the plane of the tissue was disrupted (S5B Fig). Finally, Dcp-1 staining
201 was completely absent in 40h APF retinae expressing DeIF6 in the cone cells (S5C

202 Fig) confirming a block in apoptosis. Apoptosis was then observed at 60h APF (Fig
203 5D), in line with what we observed in *GMR>DeIF6* retinae.
204 These results indicate that the expression of DeIF6 in cone cell is sufficient to alter
205 PCD and further show that aberrant PCD is one cause of the eye roughness.
206
207 **High DeIF6 levels effects are not tissue specific**
208 Once determined that the rough eye phenotype induced by DeIF6 overexpression
209 correlated with an increase in general translation and with altered PCD, we asked
210 whether such defects were specific for the eye, or a more general effect associated
211 with increased *DeIF6* gene dosage. Thus, we overexpressed DeIF6 in a different
212 epithelial organ, the wing, using the *bxMS1096GAL4* driver (*MS>DeIF6*). Such
213 manipulation led to complete disruption of the adult wing structure (Fig 6A).
214 Moreover, we performed the SUnSET assay on wing imaginal discs, and, as in eye
215 discs, we observed a two-fold increase in puromycin incorporation in *MS>DeIF6*
216 wing discs with respect to the controls (Fig 6B-C). Furthermore, DeIF6
217 overexpression in wing discs led to the presence of apoptotic cells in the dorsal
218 portion of the disc (Fig 6D).
219
220 **Gene expression analysis reveals that DeIF6 expression reshapes the**
221 **transcriptome, resulting in altered ribosome maturation and ecdysone**
222 **signalling**
223 Because it was not clear how increased translation could lead to changes in cell
224 viability, we asked whether DeIF6 was able to induce a transcriptional rewiring that
225 preceded the phenotypic effects. To this end, we performed a comprehensive gene
226 expression analysis by RNA-Seq of two distinct stages of eye development, by

227 comparing larval eye imaginal discs and pupal retinae of *GMRGAL4/+* and
228 *GMR>DeIF6* genotypes (Fig 7). At both developmental stages, in *GMR>DeIF6*
229 samples, we observed an upregulation of genes related to ribosome biogenesis (S1
230 File, Fig 7A and S6A Fig). GSAA analysis revealed also an increase in mRNAs of
231 genes involved in rRNA processing (S6A Fig). These data, together with the
232 increased puromycin incorporation before described, suggest that eIF6 is a dominant
233 inducer of ribosomal activity. Consistent with our phenotypic analysis, *GMR>DeIF6*
234 retinae displayed variations also in genes involved in eye development and in PCD
235 (Fig 7 A,C and S1 File). Notably, mRNAs encoding specialized eye enzymes, such
236 as those of pigment biosynthetic pathways, were downregulated in *GMR>DeIF6*
237 samples (S1 File), preceding the altered adult eye morphology.
238 Surprisingly, the most coordinated changes induced by DeIF6 in eye imaginal discs
239 clustered into the ecdysone pathway, with a striking downregulation of many
240 enzymes involved in 20-HydroxyEcdysone (20-HE) biosynthesis (Fig 7 A-B). For
241 example, *phm*, *sad* and *nvd* (S6B Fig) were virtually absent in *GMR>DeIF6* eye
242 imaginal disc, whereas early (*rbp*) and late (*ptp52f*) responsive genes belonging to
243 the hormone signaling cascade were downregulated (S1 File). These results indicate
244 the silencing of ecdysone pathway is one of the early events occurring upon
245 increased *DeIF6* gene dosage.
246 Chromosome organization gene sets were found upregulated in our larval GSAA
247 analysis in *GMR>DeIF6* samples (S6C Fig, S1 File), a result similar to mammalian
248 cells where eIF6 manipulation leads to changes in this set and in histone acetylation
249 (11). We found a two-fold reduction in HDACs activity in *GMR>DeIF6* adult heads
250 when compared to control (Fig 7D), in line with the observed expression changes.

251 Taken together our gene expression analysis identifies a complex rewiring of
252 transcription induced by increased dosage of eIF6 that could explain some of the
253 alterations observed.
254
255 **Ecdysone treatment or block of PCD partially rescue adult eye defects induced**
256 **by increased *DeIF6* gene dosage**
257 To understand whether the eye roughness that we observed was related to a defect
258 in PCD, experimentally observed and backed up by gene expression studies, and to
259 ecdysone signalling, predicted by gene expression studies, we administrated the
260 active form of the hormone 20-HE or we blocked PCD and evaluated the effect on
261 adult eye morphology.
262 To activate ecdysone signalling we fed *GMR>DeIF6* third instar larvae with 20-HE,
263 and we analyzed apoptosis at 40h APF and adult eye morphology. We found a
264 partial rescue of the apoptotic phenotype (Fig 7E). Indeed, immunofluorescence
265 staining for Dcp-1 showed the presence of apoptotic cells in 40h APF *GMR>DeIF6*
266 retinae treated with 20-HE, while *GMR>DeIF6* untreated retinae did not show any
267 Dcp-1 positive cell (Fig 7E). Accordingly, following 20-HE treatment, we observed a
268 partial recovery of adult eye morphology. Notably, *GMR>DeIF6* larvae fed with 20-
269 HE showed eyes 20% larger than untreated controls, although they remained
270 smaller with respect to *GMRGAL4/+* (Fig 7F).
271 To block the late PCD we co-expressed the Baculovirus caspase inhibitor p35 and
272 DeIF6, under the control of the *GMRGAL4* driver. Strikingly, we observed an almost
273 complete suppression of the rough eye phenotype (Fig 7G-H), indicating that the
274 loss of cells due the late onset of the PCD is the main cause for the alteration of
275 adult eye morphology.

276 In conclusion, these data indicate that the apoptotic defect and eye roughness
277 caused by increased *DeIF6* gene dosage depend on ecdysone signalling and on
278 dysregulated PCD.
279

280 **DISCUSSION**

281 *eIF6* gene is evolutionarily conserved and necessary for ribosome biogenesis and
282 translation. In addition, it is a single gene which is overexpressed or amplified in
283 some tumour cells (8). Our analysis in *Drosophila* confirms that eIF6 is necessary at
284 the single cell level. Moreover, ubiquitous overexpression of eIF6 is lethal at the
285 organism level in spite of the observation that overexpression of eIF6 increases
286 anabolism and protects from apoptosis at the cellular level, causing a surprisingly
287 high extent of gene modulation (Fig 8).

288 Translation is the most energy consuming process in cells (33) and thus is tightly
289 regulated, mostly at its initiation step. Recently, many studies have highlighted how
290 alterations in the ribosomal machinery and/or in translational control are involved in
291 several pathologies (34). Increased protein synthesis was often interpreted as a
292 general by-product of increased proliferation. eIF6 has been found upregulated in
293 many cancers, including mesothelioma, breast and colorectal cancer (15, 18, 35).
294 Conversely, eIF6-haploinsufficiency protects mice from lymphomagenesis in an Eμ-
295 Myc model (17). In our eIF6 overexpressing model, we observe an increase in
296 mRNAs encoding for rRNA processing factors, suggesting that ribosome biogenesis
297 is upregulated when eIF6 levels are heightened. Interestingly, we also show that the
298 overexpression of DeIF6 causes a two-fold increase in general translation both in the
299 developing eye and wing. These data show that *in vivo* eIF6 can act in a feed-
300 forward loop that amplifies the efficiency of the translational machinery.

301 How could an increase in translation dictated by excess eIF6 may impact tumour cell
302 fate? A clue to this is represented by the changes in physiological PCD in the fly eye
303 during the pupal stage (32) upon DeIF6 overexpression. A similar alteration was
304 previously observed in *X. laevis* (36). The developmental defects driven by increased

305 *DeIF6* gene dosage are consistent with two scenarios: excess DeIF6 could delay
306 developmental PCD. Alternatively, PCD could be repressed at the correct
307 developmental time and apoptotic elimination of defective cells overexpressing
308 DeIF6 could be triggered later independently of developmental signals. The fact that
309 overexpression of DeIF6 in wing discs, which are not subjected to developmental
310 apoptosis, leads to cell death supports the latter hypothesis. Overall, these
311 considerations indicate that the advantage provided by excess of eIF6 to tumour
312 cells might consist at least initially in escaping apoptotic clearance. However, the
313 following increase in apoptosis that we observe later in development is the main
314 cause of alteration of eye development, since this can be rescued by co-expression
315 of an apoptotic inhibitor. Thus, cell expressing excess DeIF6 but otherwise wild-type
316 might not resist to apoptotic elimination if not endowed by further mutations.
317 Nonetheless, there is also the possibility that the inability to remove extra-numerary
318 cells could result in a defective organogenesis, leading to aberrant apoptosis in a
319 later developmental window. On the contrary, tumours, by being intrinsically
320 disorganized, and relying on the host supply for nutrients, may therefore have an
321 advantage from eIF6 overexpression, which is always limited to the tumour and
322 absent from the surrounding stroma (35).
323 Interestingly, changes in apoptosis are mirrored in our transcriptome analysis of
324 apoptotic genes. This observation suggests that protein synthesis can acquire a
325 driver role in transcription. In this context, it is intriguing to note that increased gene
326 dosage of *eIF4E*, another rate-limiting player of translation, resulted in a similar
327 disruption of *Drosophila* eye development (37). It would be interesting to know
328 whether similar genes are affected by eIF6 and eIF4E. Thus, initiation activity is not

329 simply rate limiting for protein synthesis, but rather it is capable to affect directly or
330 indirectly specific gene expression pathways.
331 Importantly, gene expression analysis performed in the larvae reveals a strong
332 reduction of ecdysone biosynthesis and signaling. Furthermore, 20-HE treatment
333 leads to a partial rescue of the pupal apoptotic defect and consequently of the rough
334 eye phenotype. Therefore, our data place DeIF6 upstream of ecdysone regulation.
335 The precise mechanism by which eIF6 expression leads to the shut-off of ecdysone
336 biosynthetic enzymes remains to be established, but confirm the extending
337 evidences that show that translation acts upstream of metabolism (38).
338 It was intriguing to observe that DeIF6 expression leads to changes that alter
339 chromosome and chromatin organization and a decrease in HDACs activity. Thus,
340 translation factors may causes a transcriptional reshaping that could involve
341 epigenetic changes. Consistent, we previously found that, in mammals, eIF6
342 haploinsufficiency caused a gene signature that mimicked alterations obtained by
343 histones acetylation inhibitors (10). In addition, years ago a mammalian-based
344 screening for modulators of chromatin structure, surprisingly identified as a major
345 player another initiation factor, eIF3h (39). We therefore suggest that translational
346 control is, as recently proposed, a major controller of gene expression (40).
347 Remarkably, epigenetic changes have been reported to control the transcription of
348 ecdysone biosynthetic enzymes (41, 42), suggesting that alterations of
349 transcriptional regulation, perhaps at epigenetic level may be responsible for the
350 observed phenotypes.
351 In summary, our study demonstrates that overexpression of eIF6 in developing
352 organs is sufficient to induce an increase in ribosome biogenesis and translation that
353 correlates with complex transcriptional and metabolic changes leading to apoptotic

354 and hormonal defects. It will be interesting to further dissect the relationship between
355 epigenetic, metabolic, and transcriptional changes in the *Drosophila* model. Our
356 model may be useful for *in vivo* screenings of compounds that suppress the effect of
357 eIF6 overexpression in order to isolate useful therapeutics that might be relevant to
358 the protumourigenic role of mammalian eIF6, and for defining novel genetic
359 modulators of eIF6 function.
360

361 **MATERIALS AND METHODS**

362 **Genetics**

363 Fly strains were maintained on standard cornmeal food at 18°C. Genetic crosses
364 were performed at 25°C, with the exception of *GMRGAL/+* and *GMR>DeIF6*,
365 performed at 18°C. The following fly mutant stocks have been used: *GMRGAL4/CTG*
366 was a gift from Manolis Fanto (King's College, London); *UAS-DeIF6* was a gift from
367 William J Brook (Alberta Children's Hospital, Calgary) (43). Lines obtained from the
368 Bloomington Drosophila Stock Center (BDSC): *spaGAL4* (26656), *54CGAL4*
369 (27328), *w1118*, *UAS-p35* (5072), *UAS-mCD8GFP* (32184), *bxMS1096GAL4*
370 (8860).

371

372 **Mosaic analysis**

373 The *DeIF6*^{k13214} mutant clones were created by *Flippase* (*FLP*) mediated mitotic
374 recombination (25). The *DeIF6*^{k13214} *(P(w[+mC)=lacW) eIF6[k13214]ytr[k13214]) P*
375 element allele was recombined onto the right arm of chromosome two with the
376 homologous recombination site (FRT) at 42D using standard selection techniques.
377 Briefly, to create the FRT *y*$^{+}$ *pwn, DeIF6*^{k13214} chromosomes, *DeIF6*^{k13214} was
378 recombined onto the FRT chromosome originating from the *y; P{FRT}42D pwn[1]*
379 *P{y+}44B/CyO* parental stock. The *yellow*$^{+}$ *pwn DeIF6*^{k13214}*G418* resistant flies were
380 selected to create stocks for clonal analysis. Similarly, stocks used for generating
381 unmarked *DeIF6*^{k13214} clones were created by recombining *DeIF6*^{k13214} with the 42D
382 FRT chromosome using the *w[1118]; P{FRT}42D P{Ubi-GFP}2R/CyO* parental line.
383 Targeted mitotic wing clones were generated by crossing flies with *UAS-FLP*, the
384 appropriate GAL4 driver and the suitable *42D* FRT second chromosome with the
385 *42D* FRT *DeIF6*^{k13214}. The *hs* induced *DeIF6*^{k13214} mitotic clones were created by

386 following standard techniques. Briefly, 24 and 48 hours larvae with the appropriate
387 genotypes were heat shocked for 1 hour at 37°C followed by incubation at 25°C.
388

389 **Cell culture and transfections**

390 HEK293T cells were grown in DMEM (Lonza, Basel, Switzerland) supplemented with
391 10% Fetal Bovine Serum (FBS) and 1% penicillin, streptomycin, L-glutamine (Gibco,
392 Waltham, MA, USA) and maintained at 37°C and 5% CO_2. Mycoplasma testing was
393 performed before experiments. Cells were transfected with pcDNA3.1-eIF6 (44), or
394 an empty vector, with Lipofectamine® 2000 (Invitrogen, Carlsbad, CA, USA,
395 #11668019) following manufacturer protocol.
396

397 **RNA isolation and RNA sequencing**

398 Total RNA was extracted with mirVana™ isolation kit according to the manufacturer
399 protocols (ThermoFisher Scientific, Waltham, MA, USA, #AM 1560) from 10 eye
400 imaginal discs (larval stage) or 10 retinae (pupal stage). RNA quality was controlled
401 with BioAnalyzer (Agilent, Santa Clara, CA, USA). Libraries for Illumina sequencing
402 were constructed from 100 ng of total RNA with the Illumina TruSeq RNA Sample
403 Preparation Kit v2 (Set A) (Illumina, San Diego, CA, USA). The generated libraries
404 were loaded on to the cBot (Illumina) for clustering on a HiSeq Flow Cell v3. The flow
405 cell was then sequenced using a HiScanSQ (Illumina). A paired-end (2×101) run was
406 performed using the SBS Kit v3 (Illumina). Sequence deepness was at 35 million
407 reads.
408

409 **Bioinformatic Analysis**

410 *Read pre-processing and mapping*

411 Three biological replicates were analyzed for *GMRGAL4/+* and *GMR>DeIF6* larval
412 eye imaginal discs and four biological replicates were analyzed for *GMRGAL4/+* and
413 *GMR>DeIF6* pupal retinae, for a total of 14 samples. Raw reads were checked for
414 quality by FastQC software (version 0.11.2, S., A. FastQC: a quality control tool for
415 high-throughput sequence data. 2010; Available from:
416 http://www.bioinformatics.babraham.ac.uk/projects/fastqc), and filtered to remove
417 low quality calls by Trimmomatic (version 0.32) (45) using default parameters and
418 specifying a minimum length of 50. Processed reads were then aligned to *Drosophila*
419 *melanogaster* genome assembly GRCm38 (Ensembl version 79) with STAR
420 software (version 2.4.1c) (46).

421 *Gene expression quantification and differential expression analysis.*

422 HTSeq-count algorithm (version 0.6.1, option -s = no, gene annotation release 79
423 from Ensembl) (47) was employed to produce gene counts for each sample. To
424 estimate differential expression, the matrix of gene counts produced by HTSeq was
425 analyzed by DESeq2 (version DESeq2_1.12.4) (48).

426 The differential expression analysis by the DeSeq2 algorithm was performed on the
427 entire dataset composed by both larvae and pupae samples. The two following
428 comparisons were analyzed: *GMR>DeIF6 versus GMRGAL4/+* larval eye imaginal
429 discs (6 samples overall) and *GMR>DeIF6 versus GMRGAL4/+* pupal retinae (8
430 samples in total). Reads counts were normalized by calculating a size factor, as
431 implemented in DESeq2. Independent filtering procedure was then applied, setting
432 the threshold to the 62 percentile; 10886 genes were therefore tested for differential
433 expression.

434 Significantly modulated genes in *GMR>DeIF6* genotype were selected by
435 considering a false discovery rate lower than 5%.

436 Regularized logarithmic (rlog) transformed values were used for heat map
437 representation of gene expression profiles.
438 Analyses were performed in R version 3.3.1 (2016-06-21, Computing, T.R.F.f.S. R: A
439 Language and Environment for Statistical Computing. Available from: http://www.R-
440 project.org/).
441 *Functional analysis by topGO*
442 The Gene Ontology enrichment analysis was performed using topGO R
443 Bioconductor package (version topGO_2.24.0). The option *nodesize = 5* is used to
444 prune the GO hierarchy from the terms which have less than 5 annotated genes and
445 the *annFUN.db* function is used to extract the gene-to-GO mappings from the
446 genome-wide annotation library *org.Dm.eg.db* for *D. melanogaster*. The statistical
447 enrichment of GO was tested using the Fisher's exact test. Both the "classic" and
448 "elim" algorithms were used.
449 *Gene set association analysis*
450 Gene set association analysis for larvae and pupae samples was performed by
451 GSAA software (version 2.0) (49). Raw reads for 10886 genes identified by Entrez
452 Gene ID were analyzed by GSAASeqSP, using gene set C5 (*Drosophila* version
453 retrieved from http://www.go2msig.org/cgi-bin/prebuilt.cgi?taxid=7227) and
454 specifying as permutation type 'gene set' and as gene set size filtering min 15 and
455 max 800.
456
457 **Western blotting and antibodies**
458 Larval imaginal discs, pupal retinae and adult heads were dissected in cold
459 Phosphate Buffer Saline (Na_2HPO_4 10 mM, KH_2PO_4 1.8 mM, NaCl 137 mM, KCl 2.7
460 mM, pH 7.4) (PBS) and then homogenized in lysis buffer (HEPES 20 mM, KCl 100

461 mM, Glycerol 5%, EDTA pH 8.0 10 mM, Triton-X 0.1%, DTT 1mM) freshly
462 supplemented with Protease Inhibitors (Sigma, St. Louis, MO, USA, #P8340).
463 Protein concentration was determined by BCA analysis (Pierce, Rockford, IL, USA,
464 #23227). Equal amounts of proteins were loaded and separated on a 10% SDS-
465 PAGE, then transferred to a PVDF membrane. Membranes were blocked in 10%
466 Bovine Serum Albumin (BSA) in PBS-Tween (0.01%) for 30 minutes at 37°C. The
467 following primary antibodies were used: rabbit anti-eIF6 (1:500, this study), rabbit
468 anti-β-actin (1:4000, CST, Danvers, MA, USA, #4967). To produce the anti-eIF6
469 antibody used in this study, a rabbit polyclonal antiserum against two epitopes on
470 COOH-terminal peptide of eIF6 (NH2-CLSFVGMNTTATEI-COOH eIF6 203-215 aa;
471 NH2-CATVTTKLRAALIEDMS-COOH eIF6 230-245 aa) was prepared by
472 PrimmBiotech (Milan, Italy, Ab code: 201212-00003 GHA/12), purified in a CNBr-
473 Sepharose column and tested for its specificity against a mix of synthetic peptides
474 with ELISA test. The following secondary antibodies were used: donkey anti-mouse
475 IgG HRP (1:5000, GE Healthcare, Little Chalfont, UK, Amersham #NA931) and
476 donkey anti-rabbit IgG HRP (1:5000, GE Healthcare, Amersham #NA934).

477

478 **SUnSET Assay**

479 Larval imaginal eye and wing discs were dissected in complete Schneider medium
480 (Lonza, Basel, Switzerland) and treated *ex vivo* with puromycin (50 µg/mL) for 30
481 minutes at room temperature, then fixed in 3% paraformaldehyde (PFA) for 1 hour at
482 room temperature. Immunofluorescences were then performed as described below,
483 using a mouse anti Puromycin (1:500, Merck Millipore, Billerica, MA, USA,
484 #MABE343) as a primary antibody. Discs were then examined by confocal
485 microscope (Leica SP5, Leica, Wetzlar, Germany) and fluorescence intensity was

486 measured with ImageJ software. For protein synthesis measurement in HEK293T
487 cells, after 48 hours of transfection with the pcDNA3.1-eIF6 or the empty vector, we
488 followed the adapted SUnSET protocol described in (50).
489
490 **Cells count**
491 *GMRGAL4/+* and *GMR>DeIF6* pupal retinae at 40h APF were dissected, fixed, and
492 stained with anti-Armadillo to count cells, as previously described (51). Cells
493 contained within a hexagonal array (an imaginary hexagon that connects the centres
494 of the surrounding six ommatidia) were counted; for different genotypes, the number
495 of cells per hexagon was calculated by counting cells, compared with corresponding
496 control. Cells at the boundaries between neighbouring ommatidia count half. At least
497 3 hexagons (equivalent to 9 full ommatidia) were counted for each genotype, and
498 phenotypes were analysed. Standard Deviation (SD) was used as statistical analysis.
499
500 **Immunofluorescences, antibodies and TUNEL Assay**
501 Larval imaginal discs and pupal retinae were dissected in cold PBS and fixed in 3%
502 paraformaldehyde (PFA) for 1 hour at room temperature, then washed twice with
503 PBS and blocked in PBTB (PBS, Triton 0.3%, 5% Normal Goat Serum and 2%
504 Bovine Serum Albumin) for 3 hours at room temperature. Primary antibodies were
505 diluted in PBTB solution and incubated O/N at 4°C. After three washes with PBS,
506 tissues were incubated O/N at 4°C with secondary antibodies and DAPI (1:1000,
507 Molecular Probes, Eugene, OR, USA, #D3571) in PBS. After three washes with PBS,
508 eye imaginal discs and retinae were mounted on slides with ProLong Gold
509 (LifeTechnologies, Carlsbad, CA, USA, #P36930). The following primary antibodies
510 were used: rabbit anti-eIF6 (1:50, this study), rat anti-ELAV (1:100, Developmental

511 Study Hybridoma Bank DSHB, Iowa City, IA, USA, #7E8A10), mouse anti-CUT
512 (1:100, DSHB, #2B10), mouse anti-Rough (1:100, DSHB, #ro-62C2A8), mouse anti-
513 Armadillo (1:100, DSHB, #N27A), mouse anti-Chaoptin (1:100, DSHB, #24B10),
514 rabbit anti- Dcp-1 (1:50, CST, #9578), mouse anti-Puromycin (1:500, Merck Millipore,
515 #MABE343). The following secondary antibodies were used: donkey anti-rat, donkey
516 anti-mouse, donkey anti-rabbit (1:500 Alexa Fluor® secondary antibodies, Molecular
517 Probes). Dead cells were detected using the In Situ Cell Death Detection Kit TMR
518 Red (Roche, Basel, Switzerland, #12156792910) as manufacturer protocol, with
519 some optimization. Briefly, retinae of the selected developmental stage were
520 dissected in cold PBS and fixed with PFA 3% for 1 hour at room temperature. After
521 three washes in PBS, retinae were permeabilized with Sodium Citrate 0.1%-Triton-X
522 0.1% for 2 minutes at 4°C and then incubated overnight at 37°C with the enzyme mix.
523 Retinae were then rinsed three times with PBS, incubated with DAPI to stain nuclei
524 and mounted on slides. Discs and retinae were examined by confocal microscopy
525 (Leica SP5) and analysed with Volocity 6.3 software (Perkin Elmer, Waltham, MA,
526 USA).
527
528 **Semithin sections**
529 Semithin sections were prepared as described in (52). Adult eyes were fixed in 0.1 M
530 Sodium Phosphate Buffer, 2% glutaraldehyde, on ice for 30 min, then incubated with
531 2% OsO4 in 0.1 M Sodium Phosphate Buffer for 2 hours on ice, dehydrated in
532 ethanol (30%, 50%, 70%, 90%, and 100%) and twice in propylene oxide. Dehydrated
533 eyes were then incubated O/N in 1:1 mix of propylene oxide and epoxy resin (Sigma,
534 Durcupan™ ACM). Finally, eyes were embedded in pure epoxy resin and baked O/N
535 at 70°C. The embedded eyes were cut on a Leica UltraCut UC6 microtome using a

536 glass knife and images were acquired with a 100X oil lens, Nikon Upright XP61
537 microscope (Nikon, Tokyo, Japan).
538
539 **Ecdysone treatment**
540 For ecdysone treatment, 20-HydroxyEcdysone (20HE) (Sigma, #H5142) was
541 dissolved in 100% ethanol to a final concentration of 5 mg/mL; third instar larvae
542 from different genotypes (*GMRGAL4/+* and *GMR>DeIF6*) were collected and placed
543 in individual vials on fresh standard cornmeal food supplemented with 240 µg/mL 20-
544 HE. Eye phenotype was analyzed in adult flies, and images were captured with a
545 TOUPCAM™ Digital camera. Eye images were analyzed with ImageJ software.
546
547 ***In vitro* Ribosome Interaction Assay (iRIA)**
548 iRIA assay was performed as described in (30). Briefly, 96-well plates were coated
549 with a cellular extract diluted in 50 µL of PBS, 0.01% Tween-20, O/N at 4°C in humid
550 chamber. Coating solution was removed and aspecific sites were blocked with 10%
551 BSA, dissolved in PBS, 0.01% Tween-20 for 30 minutes at 37 °C. Plates were
552 washed with 100 µL/well with PBS-Tween. 0.5 µg of recombinant biotinylated eIF6
553 were resuspended in a reaction mix: 2.5 mM $MgCl_2$, 2% DMSO and PBS-0.01%
554 Tween, to reach 50 µL of final volume/well, added to the well and incubated with
555 coated ribosomes for 1 hour at room temperature. To remove unbound proteins,
556 each well was washed 3 times with PBS, 0.01% Tween-20. HRP-conjugated
557 streptavidin was diluted 1:7000 in PBS, 0.01% Tween-20 and incubated in the well,
558 30 minutes at room temperature, in a final volume of 50 µL. Excess of streptavidin
559 was removed through three washes with PBS-Tween. OPD (o-phenylenediamine
560 dihydrochloride) was used according to the manufacturer's protocol (Sigma-Aldrich)

561 as a soluble substrate for the detection of streptavidin peroxidase activity. The signal
562 was detected after the incubation, plates were read at 450 nm on a multiwell plate
563 reader (Microplate model 680, Bio-Rad, Hercules, CA, USA).
564
565 **HDACs activity**
566 HDACs activity was measured with the fluorometric HDAC Activity Assay kit (Sigma,
567 #CS1010-1KT) according to the manufacturer's instructions. Briefly, cells were lysed
568 with a buffer containing 50 mM HEPES, 150 mM NaCl, and 0.1% Triton X-100
569 supplemented with fresh protease inhibitors. 20 µg of cell lysates were incubated
570 with assay buffer containing the HDACs substrate for 30 minutes at 30°C. The
571 reaction was terminated, and the fluorescence intensity was measured in a
572 fluorescence plate reader with Ex. = 350-380 nm and Em. = 440-460 nm.
573
574 **Statistical Analysis**
575 Each experiment was repeated at least three times, as biological replicates; means
576 and standard deviations between different experiments were calculated. Statistical *p*-
577 values obtained by Student *t-test* were indicated: three asterisks *** for *p*-values less
578 than 0.001, two asterisks ** for *p*-values less than 0.01 and one asterisks * for *p*-
579 values less than 0.05.
580
581 **ACCESSION NUMBER**
582 ArrayExpress ID will be provided upon acceptance for publication.
583
584 **SUPPLEMENTARY DATA**

585 Supplementary Data will be available on ----- online. For review, Supplementary
586 Figures and Supplementary Files are available.
587
588 **FUNDING**

589 This work was supported by ERC TRANSLATE 338999 and FONDAZIONE
590 CARIPLO to SB.
591
592 **ACKNOWLEDGEMENTS**

593 We thank William Brook (Alberta Children's Hospital, Calgary) for UASDeIF6 stocks
594 and Manolis Fanto (King's College, London) for stocks and suggestions. We thank
595 Valeria Berno for imaging help and Vera Giulia Volpi for semithin sections
596 preparation.
597 The authors declare no competing interests.
598
599 **REFERENCES**

600 1. Hershey JW, Sonenberg N, Mathews MB. Principles of translational control: an overview.
601 Cold Spring Harb Perspect Biol. 2012 Dec 01;4(12).
602 2. Kressler D, Hurt E, Bassler J. A Puzzle of Life: Crafting Ribosomal Subunits. Trends Biochem
603 Sci. 2017 Aug;42(8):640-54.
604 3. Kressler D, Linder P, de La Cruz J. Protein trans-acting factors involved in ribosome
605 biogenesis in Saccharomyces cerevisiae. Mol Cell Biol. 1999 Dec;19(12):7897-912.
606 4. Venema J, Tollervey D. Ribosome synthesis in Saccharomyces cerevisiae. Annu Rev Genet.
607 1999;33:261-311.
608 5. Warner JR, Vilardell J, Sohn JH. Economics of ribosome biosynthesis. Cold Spring Harb Symp
609 Quant Biol. 2001;66:567-74.

610 6. Robichaud N, Sonenberg N. Translational control and the cancer cell response to stress. Curr
611 Opin Cell Biol. 2017 Apr;45:102-9.
612 7. Miluzio A, Beugnet A, Volta V, Biffo S. Eukaryotic initiation factor 6 mediates a continuum
613 between 60S ribosome biogenesis and translation. EMBO Rep. 2009 May;10(5):459-65.
614 8. Brina D, Miluzio A, Ricciardi S, Biffo S. eIF6 anti-association activity is required for ribosome
615 biogenesis, translational control and tumor progression. Biochim Biophys Acta. 2015
616 Jul;1849(7):830-5.
617 9. Gandin V, Miluzio A, Barbieri AM, Beugnet A, Kiyokawa H, Marchisio PC, et al. Eukaryotic
618 initiation factor 6 is rate-limiting in translation, growth and transformation. Nature. 2008 Oct
619 02;455(7213):684-8.
620 10. Brina D, Miluzio A, Ricciardi S, Clarke K, Davidsen PK, Viero G, et al. eIF6 coordinates insulin
621 sensitivity and lipid metabolism by coupling translation to transcription. Nat Commun. 2015 Sep
622 18;6:8261.
623 11. Miluzio A, Ricciardi S, Manfrini N, Alfieri R, Oliveto S, Brina D, et al. Translational control by
624 mTOR-independent routes: how eIF6 organizes metabolism. Biochem Soc Trans. 2016 Dec
625 15;44(6):1667-73.
626 12. Ceci M, Gaviraghi C, Gorrini C, Sala LA, Offenhauser N, Marchisio PC, et al. Release of eIF6
627 (p27BBP) from the 60S subunit allows 80S ribosome assembly. Nature. 2003 Dec 04;426(6966):579-
628 84.
629 13. Biffo S, Sanvito F, Costa S, Preve L, Pignatelli R, Spinardi L, et al. Isolation of a novel beta4
630 integrin-binding protein (p27(BBP)) highly expressed in epithelial cells. J Biol Chem. 1997 Nov
631 28;272(48):30314-21.
632 14. Donadini A, Giodini A, Sanvito F, Marchisio PC, Biffo S. The human ITGB4BP gene is
633 constitutively expressed in vitro, but highly modulated in vivo. Gene. 2001 Mar 21;266(1-2):35-43.
634 15. Miluzio A, Oliveto S, Pesce E, Mutti L, Murer B, Grosso S, et al. Expression and activity of eIF6
635 trigger malignant pleural mesothelioma growth in vivo. Oncotarget. 2015 Nov 10;6(35):37471-85.

636 16. Sanvito F, Piatti S, Villa A, Bossi M, Lucchini G, Marchisio PC, et al. The beta4 integrin
637 interactor p27(BBP/eIF6) is an essential nuclear matrix protein involved in 60S ribosomal subunit
638 assembly. J Cell Biol. 1999 Mar 08;144(5):823-37.
639 17. Miluzio A, Beugnet A, Grosso S, Brina D, Mancino M, Campaner S, et al. Impairment of
640 cytoplasmic eIF6 activity restricts lymphomagenesis and tumor progression without affecting normal
641 growth. Cancer Cell. 2011 Jun 14;19(6):765-75.
642 18. Gatza ML, Silva GO, Parker JS, Fan C, Perou CM. An integrated genomics approach identifies
643 drivers of proliferation in luminal-subtype human breast cancer. Nat Genet. 2014 Oct;46(10):1051-9.
644 19. Brand AH, Perrimon N. Targeted gene expression as a means of altering cell fates and
645 generating dominant phenotypes. Development. 1993 Jun;118(2):401-15.
646 20. del Valle Rodriguez A, Didiano D, Desplan C. Power tools for gene expression and clonal
647 analysis in Drosophila. Nat Methods. 2011 Dec 28;9(1):47-55.
648 21. Kumar JP. Building an ommatidium one cell at a time. Dev Dyn. 2012 Jan;241(1):136-49.
649 22. Cagan RL, Reh TA. Preface. Aspects of eye development: advances over the past twenty
650 years. Curr Top Dev Biol. 2010;93:xi-xii.
651 23. Ready DF, Hanson TE, Benzer S. Development of the Drosophila retina, a neurocrystalline
652 lattice. Dev Biol. 1976 Oct 15;53(2):217-40.
653 24. Spradling AC, Stern D, Beaton A, Rhem EJ, Laverty T, Mozden N, et al. The Berkeley
654 Drosophila Genome Project gene disruption project: Single P-element insertions mutating 25% of
655 vital Drosophila genes. Genetics. 1999 Sep;153(1):135-77.
656 25. Harrison DA, Perrimon N. Simple and efficient generation of marked clones in Drosophila.
657 Curr Biol. 1993 Jul 01;3(7):424-33.
658 26. Basler K, Hafen E. Specification of cell fate in the developing eye of Drosophila. Bioessays.
659 1991 Dec;13(12):621-31.

660 27. Tomlinson A, Bowtell DD, Hafen E, Rubin GM. Localization of the sevenless protein, a
661 putative receptor for positional information, in the eye imaginal disc of Drosophila. Cell. 1987 Oct
662 09;51(1):143-50.
663 28. Tomlinson A, Kimmel BE, Rubin GM. rough, a Drosophila homeobox gene required in
664 photoreceptors R2 and R5 for inductive interactions in the developing eye. Cell. 1988 Dec
665 02;55(5):771-84.
666 29. Van Vactor DL, Jr., Cagan RL, Kramer H, Zipursky SL. Induction in the developing compound
667 eye of Drosophila: multiple mechanisms restrict R7 induction to a single retinal precursor cell. Cell.
668 1991 Dec 20;67(6):1145-55.
669 30. Pesce E, Minici C, Babetaler J, Hurt E, Degano M, Calamita P, et al. Direct and high
670 throughput (HT) interactions on the ribosomal surface by iRIA. Sci Rep. 2015 Oct 21;5:15401.
671 31. Schmidt EK, Clavarino G, Ceppi M, Pierre P. SUnSET, a nonradioactive method to monitor
672 protein synthesis. Nat Methods. 2009 Apr;6(4):275-7.
673 32. Rusconi JC, Hays R, Cagan RL. Programmed cell death and patterning in Drosophila. Cell
674 Death Differ. 2000 Nov;7(11):1063-70.
675 33. Buttgereit F, Brand MD. A hierarchy of ATP-consuming processes in mammalian cells.
676 Biochem J. 1995 Nov 15;312 (Pt 1):163-7.
677 34. Shenoy N, Kessel R, Bhagat TD, Bhattacharyya S, Yu Y, McMahon C, et al. Alterations in the
678 ribosomal machinery in cancer and hematologic disorders. J Hematol Oncol. 2012 Jun 18;5:32.
679 35. Sanvito F, Vivoli F, Gambini S, Santambrogio G, Catena M, Viale E, et al. Expression of a
680 highly conserved protein, p27BBP, during the progression of human colorectal cancer. Cancer Res.
681 2000 Feb 01;60(3):510-6.
682 36. De Marco N, Iannone L, Carotenuto R, Biffo S, Vitale A, Campanella C. p27(BBP)/eIF6 acts as
683 an anti-apoptotic factor upstream of Bcl-2 during Xenopus laevis development. Cell Death Differ.
684 2010 Feb;17(2):360-72.

685 37. Hernandez G, Altmann M, Sierra JM, Urlaub H, Diez del Corral R, Schwartz P, et al. Functional
686 analysis of seven genes encoding eight translation initiation factor 4E (eIF4E) isoforms in Drosophila.
687 Mech Dev. 2005 Apr;122(4):529-43.
688 38. Biffo S, Manfrini N, Ricciardi S. Crosstalks between translation and metabolism in cancer.
689 Curr Opin Genet Dev. 2017 Nov 15;48:75-81.
690 39. Daxinger L, Oey H, Apedaile A, Sutton J, Ashe A, Whitelaw E. A forward genetic screen
691 identifies eukaryotic translation initiation factor 3, subunit H (eIF3h), as an enhancer of variegation
692 in the mouse. G3 (Bethesda). 2012 Nov;2(11):1393-6.
693 40. Schwanhausser B, Busse D, Li N, Dittmar G, Schuchhardt J, Wolf J, et al. Global quantification
694 of mammalian gene expression control. Nature. 2011 May 19;473(7347):337-42.
695 41. Borsos BN, Pankotai T, Kovacs D, Popescu C, Pahi Z, Boros IM. Acetylations of Ftz-F1 and
696 histone H4K5 are required for the fine-tuning of ecdysone biosynthesis during Drosophila
697 metamorphosis. Dev Biol. 2015 Aug 01;404(1):80-7.
698 42. Pankotai T, Popescu C, Martin D, Grau B, Zsindely N, Bodai L, et al. Genes of the ecdysone
699 biosynthesis pathway are regulated by the dATAC histone acetyltransferase complex in Drosophila.
700 Mol Cell Biol. 2010 Sep;30(17):4254-66.
701 43. Ji Y, Shah S, Soanes K, Islam MN, Hoxter B, Biffo S, et al. Eukaryotic initiation factor 6
702 selectively regulates Wnt signaling and beta-catenin protein synthesis. Oncogene. 2008 Jan
703 31;27(6):755-62.
704 44. Benelli D, Cialfi S, Pinzaglia M, Talora C, Londei P. The translation factor eIF6 is a Notch-
705 dependent regulator of cell migration and invasion. PLoS One. 2012;7(2):e32047.
706 45. Bolger AM, Lohse M, Usadel B. Trimmomatic: a flexible trimmer for Illumina sequence data.
707 Bioinformatics. 2014 Aug 1;30(15):2114-20.
708 46. Dobin A, Davis CA, Schlesinger F, Drenkow J, Zaleski C, Jha S, et al. STAR: ultrafast universal
709 RNA-seq aligner. Bioinformatics. 2013 Jan 01;29(1):15-21.

710 47. Anders S, Pyl PT, Huber W. HTSeq--a Python framework to work with high-throughput
711 sequencing data. Bioinformatics. 2015 Jan 15;31(2):166-9.
712 48. Love MI, Huber W, Anders S. Moderated estimation of fold change and dispersion for RNA-
713 seq data with DESeq2. Genome Biol. 2014;15(12):550.
714 49. Xiong Q, Mukherjee S, Furey TS. GSAASeqSP: a toolset for gene set association analysis of
715 RNA-Seq data. Sci Rep. 2014;4:6347.
716 50. Calamita P, Miluzio A, Russo A, Pesce E, Ricciardi S, Khanim F, et al. SBDS-Deficient Cells Have
717 an Altered Homeostatic Equilibrium due to Translational Inefficiency Which Explains their Reduced
718 Fitness and Provides a Logical Framework for Intervention. PLoS Genet. 2017 Jan;13(1):e1006552.
719 51. Cordero J, Jassim O, Bao S, Cagan R. A role for wingless in an early pupal cell death event
720 that contributes to patterning the Drosophila eye. Mech Dev. 2004 Dec;121(12):1523-30.
721 52. Montrasio S, Mlodzik M, Fanto M. A new allele uncovers the role of echinus in the control of
722 ommatidial rotation in the Drosophila eye. Dev Dyn. 2007 Oct;236(10):2936-42.
723
724
725

726 **FIGURES LEGENDS**

727 **Fig 1. Increased DeIF6 levels in the developing eye result in a rough eye**
728 **phenotype, reduced free 60S, and increased translation. (A)** Stereomicroscope
729 images of *GMRGAL4/+* and *GMR>DeIF6* eyes, showing a noteworthy rough eye
730 phenotype. **(B)** Representative western blot showing the levels of DeIF6 expression
731 in *GMRGAL4/+* and *GMR>DeIF6* adult eyes. **(C)** Representative SEM images of
732 *GMRGAL4/+* and *GMR>DeIF6* adult eyes. DeIF6 overexpressing eyes have an
733 aberrant morphology, showing flattened ommatidia and randomly arranged bristles.
734 Scale bar, respectively for A-C, 10 µm, 5 µm, 2.5 µm **(D)** Representative tangential
735 sections of *GMRGAL4/+* and *GMR>DeIF6* adult eyes indicating that photoreceptors
736 are still present in *GMR>DeIF6* eyes, even if their arrangement is lost. Scale bar 10
737 µm. **(E)** iRIA assay showing that DeIF6 increased dosage reduce the number of free
738 60S subunits, *in vivo* **(F)** Quantification of SUnSET assay using ImageJ software.
739 Graph represents mean ± SD. Statistic applied was *t-test*, paired, two tails. **(G)**
740 Representative SUnSET assay performed using immunofluorescence experiments,
741 indicating a two-fold increase in general translation when DeIF6 levels are increased
742 in eye imaginal discs. Scale bar 10 µm.

743

744 **Fig 2. *GMR>DeIF6* retinae retain cell identity but show an aberrant morphology.**
745 **(A)** Mid-pupal stage retinae (40h APF) stained for eIF6 confirming protein expression.
746 **(B)** Staining for ELAV (neuronal cells marker) and Cut (cone cells marker) showing
747 that both neurons and cone cells retain their identity. Noteworthy, neural and cone
748 cells show an incorrect arrangement on the plane in association with increased
749 DeIF6 levels. **(C)** Chaoptin (intra-photoreceptor membranes marker) staining
750 confirms the aberrant morphology of *GMR>DeIF6* retinae. Scale bar 10 µm.

751

752 **Fig 3. The apoptotic wave is delayed when *DeIF6* gene dosage is increased. (A)**
753 Mid-pupal stage retinae (40h APF) stained for the *Drosophila* caspase Dcp-1.
754 *GMRGAL4/+* retinae show Dcp-1 positive cells, indicating that PCD is ongoing at this
755 developmental stage. On the contrary, *GMR>DeIF6* retinae do not show Dcp-1
756 positive cells, indicating a block in PCD. **(B)** Late-pupal stage (60h APF) retinae
757 stained for the *Drosophila* caspase Dcp-1. *GMRGAL4/+* retinae show the absence of
758 Dcp-1 positive cells, as expected (PCD already finished at this developmental stage).
759 On the contrary, *GMR>DeIF6* retinae, show Dcp-1 positive cells, indicating a delay in
760 PCD associated to more DeIF6 levels. **(C)** Dcp-1 positive cells counts indicate an
761 overall delay and increase in PCD when *DeIF6* gene dosage is increased during eye
762 development. Graph represents mean ± SD. Statistic applied was *t-test*, paired, two
763 tails. Scale bar 10 µm.

764

765 **Fig 4. Cell number is altered during pupal stage in *GMR>DeIF6*. (A)** Mid-pupal
766 stage (40h APF) retinae stained for Armadillo, the *Drosophila* β-catenin homologue,
767 showing that when DeIF6 is increased there are extra-numerary cells (indicated as *)
768 around each ommatidium. **(B)** Late-pupal stage (60h APF) retinae stained for
769 Armadillo, showing the loss of all cells around ommatidia upon DeIF6
770 overexpression. Scale bar 10 µm.

771

772 **Fig 5. A specific increase of *DeIF6* gene dosage in cone cells results in a rough**
773 **eye phenotype. (A-B)** Overexpression of DeIF6 in cone cells results in rough eye
774 phenotype. **(A)** Representative stereomicroscope images of *spaGAL4/+* and
775 *spa>DeIF6* eyes showing a rough eye phenotype. **(B)** Representative tangential

776 semithin sections of *spaGAL4/+* and *spa>DeIF6* adult eyes showing disruption of the
777 structure upon DeIF6 overexpression in cone cells. **(C)** Mid-pupal stage (40h APF)
778 retinae stained for eIF6 confirming that overexpression of DeIF6 is restricted only to
779 cone cells. **(D)** Late-pupal stage (60h APF) retinae of *spaGAL4/+* and *spa>DeIF6*
780 genotypes stained for Dcp-1 confirming the delayed and increased apoptosis already
781 observed in *GMR>DeIF6* flies. (C-D) Scale bar 10 µm.
782
783 **Fig 6. Altered *DeIF6* gene dosage affects the wing. (A)** Adult wings *MS>DeIF6*
784 have a completely aberrant phenotype. **(B)** SUnSET assay quantification of an
785 immunofluorescence experiment, indicating again a two-fold increase in general
786 translation when in *MS>DeIF6* wing discs. Graph represents mean ± SD. Statistic
787 applied was *t-test*, paired, two tails. **(C)** Representative SUnSET assay performed
788 using immunofluorescence experiment, indicating again a two-fold increase in
789 general translation when in *MS>DeIF6* wing discs. For each genotype, two
790 magnifications are compared: 63x (scale bar 50 µm) and, in the small squares, 252x
791 (scale bar 10 µm). **(D)** Apoptosis is increased in *MS>DeIF6* wing imaginal disc. Wing
792 discs stained for Dcp-1 and DeIF6 in control flies (*MSGAL4/+*) and in in *MS>DeIF6*.
793 In *MS>DeIF6* there is a striking increase in apoptotic events, compared to the control.
794 Scale bar 50 µm.
795
796 **Fig 7. DeIF6 induces a reshaping of transcription, resulting in rRNA processing**
797 **alteration and in a gene signature specific for the eye, unveiling a role of 20-HE**
798 **in defective apoptosis. (A)** Venn Diagram indicating genes differentially expressed
799 in *GMR>DeIF6* larval eye imaginal discs and *GMR>DeIF6* retinae with respect to
800 controls (*GMRGAL4/+).* **(B)** The Ecdysone Biosynthetic Pathway is shut off when

801 DeIF6 is upregulated. Heat Map representing absolute gene expression levels in
802 *GMR>DeIF6* and *GMRGAL4/+* eye imaginal disc samples for the subset of gene
803 sets involved in Ecdysone Biosynthesis by Gene Ontology analysis. **(C)** mRNAs
804 involved in Programmed Cell Death and in Eye Differentiation are upregulated in
805 *GMR>DeIF6* retinae. Heat Map representing absolute gene expression levels in
806 *GMR>DeIF6* and *GMRGAL4/+* retinae samples for the subset of gene sets involved
807 in Programmed Cell Death and Eye Differentiation by Gene Ontology Analysis. **(D)**
808 High levels of DeIF6 are associated to lower HDAC activity. Representative graph
809 showing a lower HDACs activity in association to high DeIF6 protein levels. The
810 assay has been performed on total protein extracts from *GMRGAL4/+* and
811 *GMR>DeIF6* adult heads. **(E-F)** 20-HE treatment partially rescue the rough eye
812 phenotype and the delay in apoptosis in 40h APF retinae **(E)** Immunofluorescence
813 images showing that 20-HE treatment (240 µg/mL in standard fly food) rescues the
814 apoptotic delay observed in *GMR>DeIF6* 40h APF retinae. **(F)** Representative graph
815 showing the *GMR>DeIF6* adult fly eye size with or without treatment with 20-HE. As
816 indicated in the graph, the fly eye size is partially rescued when the hormone is
817 added to the fly food. Graphs represent mean ± SD. Statistic applied was *t-test*,
818 paired, two tails. **(G-H)** Blocking apoptosis rescues the rough eye phenotype. **(G)**
819 Representative stereomicroscope images of *GMR>DeIF6; p35* and *GMR>DeIF6*
820 adult eyes. **(H)** Western blot showing eIF6 levels in *GMR>DeIF6; p35* and
821 *GMR>DeIF6* eyes. For each genotype, the densitometric ratio (DeIF6/β-actin) was
822 analysed with ImageJ and reported.
823
824 **Fig 8. Model for eIF6 function.** We demonstrated that increased levels of eIF6 are
825 associated to increased general translation, resulting in a transcription rewiring.

826 RNASeq analysis confirms that altering *DeIF6* gene dosage modulates apoptosis
827 during development and interestingly, reveals a shutdown of genes involved in 20-
828 HydroxyEcdysone biosynthesis. In addition, we found an upregulation of genes
829 related to chromatin organization.
830
831 **S1 Fig. Strong alteration of *DeIF6* gene dosage is incompatible with life and is**
832 **associated with increased general translation when overexpressed in**
833 **mammalian cells. (A)** *DeIF6*^{k13214} mosaic analysis. (A-F) Wild type (Oregon R) wing
834 margin and *DeIF6* mutant clones. (A and B) Wild type control anterior wing margin.
835 (C and D) Wing margin clones induced in *Minute/DeIF6*^{k13214} flies according the
836 crosses outlined in Materials and Methods. (E and F) Mutant clones induced along
837 the wing margin by using UA*S-Flp*; *C96*-GAL4; FRT *DeIF6*^{k13214}/FRT *y+ pwn* flies. (D
838 and F) Arrows and arrowheads indicate *pwn DeIF63214* homozygous mutant and
839 heterozygous *Minute* (*M/pwn DeIF6*^{k13214}) tissues, respectively. Asterisks denote *y*
840 twin cells and the "^" highlights heterozygous wild type bristles. **(B)** Ectopic
841 embryonic *DeIF6* phenotypes. (A-B) Embryonic cuticle preparations in *TubGAL4/+*
842 (A) and *Tub>DeIF6* (B) evidencing that DeIF6 gain of function is embryonic lethal.
843 **(C-E)** eIF6 overexpression results in translation increase in mammalian cells. **(C)**
844 Representative western blot showing the levels of DeIF6 expression in empty vector-
845 and eIF6-pcDNA3.1 transfected cells. **(D)** SUnSET assay quantification of FACS
846 analysis performed on HEK293T cells showing the same increase in general
847 translation observed in *Drosophila* eye imaginal discs. Graph represents mean ± SD.
848 Statistic applied was *t-test*, paired, two tails. **(E)** Dot plot of FACS analysis performed
849 in HEK293T cells of overexpressing and control cells' populations.
850

851 **S2 Fig. *GMR>DeIF6* eye imaginal discs retain cell identity and morphology. (A)**
852 *GMR>DeIF6* and *GMRGAL4/+* eye imaginal discs stained for eIF6 confirm the
853 protein overexpression. **(B)** *GMR>DeIF6* and *GMRGAL4/+* eye imaginal discs
854 stained for ELAV and Cut show that both neurons and cone cells preserve their
855 identities. **(C)** *GMR>DeIF6* and *GMRGAL4/+* eye imaginal discs stained for Rough
856 (R2-R5 marker) show the same pattern in both genotypes. Scale bar 50 μm.
857
858 **S3 Fig. PCD is delayed when *DeIF6* gene dosage is increased.** TUNEL assay on
859 early (28h APF) **(A)** and mid-pupal (40h APF) stages **(B)** retinae indicate that PCD is
860 blocked at these developmental stages when DeIF6 is overexpressed. Scale bar 50
861 μm.
862
863 **S4 Fig. Cell number is altered in *GMR>DeIF6* retinae. (A)** Comparison of cells
864 number across two genotypes, *GMRGAL4/+* and *GMR>DeIF6*, shows that there is
865 an increase in *GMR>DeIF6* with respect to control. 'Δ cells per ommatidium' refers to
866 the number of cells gained or lost within a ommatidia (number of cells in hexagon
867 divided by 3). Results in the third column represent the mean ± SD. **(B)** Late-pupal
868 stage (72h APF) retinae stained for Armadillo, the *Drosophila* β-catenin homologue,
869 showing that when DeIF6 is overexpressed cells around ommatidia are lost. Scale
870 bar 10 μm.
871
872 **S5 Fig. Increasing *DeIF6* gene dosage only in pigment cells or in cone cells**
873 **results in a rough eye phenotype and in an aberrant morphology associated**
874 **with a block in apoptosis (A)** Overexpression of DeIF6 only in pigment cells results
875 in rough eye phenotype. **(B)** Mid-pupal stage (40h APF) retinae of *spaGAL4/+* and

876 *spa>DeIF6* genotypes stained for ELAV and CUT confirm that neural and cone cell
877 identity is retained, whereas cell arrangement is altered. **(C)** Mid-pupal stage (40h
878 APF) retinae of *spaGAL4/+* and *spa>DeIF6* genotypes stained for Dcp-1 confirm the
879 block in apoptosis already demonstrated in *GMR>DeIF6* flies. Scale bar 10 µm.
880
881 **S6 Fig. RNASeq analysis reveals an upregulation in genes belonging to**
882 **ribosome biogenesis and chromosome organization gene sets and a strong**
883 **downregulation of genes related to 20-HydroxyEcdysone biosynthesis. (A)**
884 Gene Set Association Analysis (GSAA) indicates a significative upregulation of
885 ribosomal machinery. Representative Enrichment Plots indicating a striking
886 upregulation of genes involved in rRNA Processing and Ribosome Biogenesis in
887 both *GMR>DeIF6* eye imaginal discs and *GMR>DeIF6* retinae with respect to their
888 controls (*GMRGAL4/+).* **(B)** 20-HydroxyEcdysone biosynthetic pathway scheme.
889 Genes involved in 20-HE biosynthesis are strongly downregulated in *GMR>DeIF6*
890 eye imaginal disc, with respect to control. **(C)** GSAA shows an upregulation of genes
891 related to chromosome organization gene set in *GMR>DeIF6* eye imaginal disc, with
892 respect to control.
893

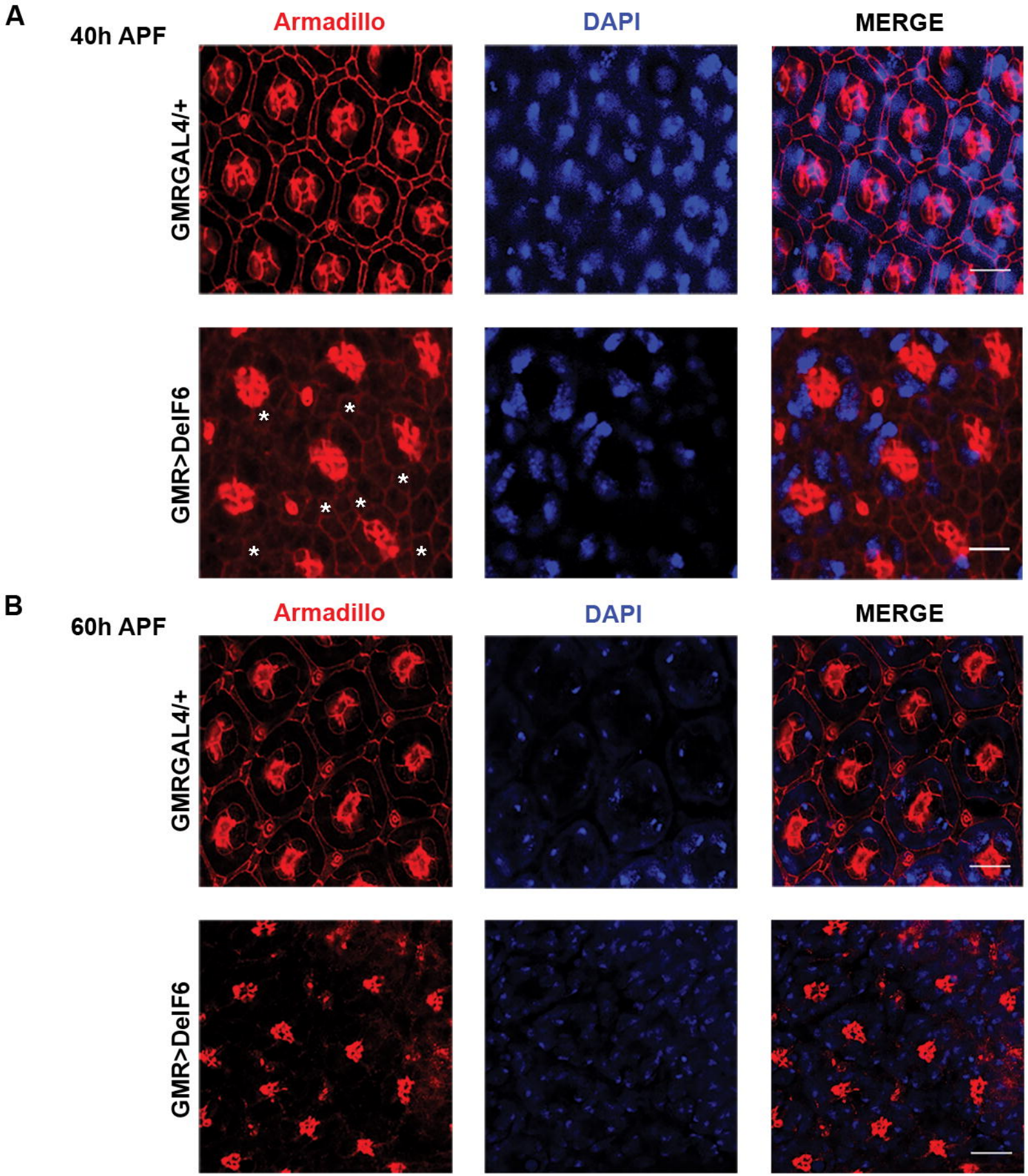
A
40h APF
Armadillo
DAPI
MERGE
GMRGAL4/+
GMR>DeIF6
B
60h APF
Armadillo
DAPI
MERGE
GMRGAL4/+
GMR>DeIF6

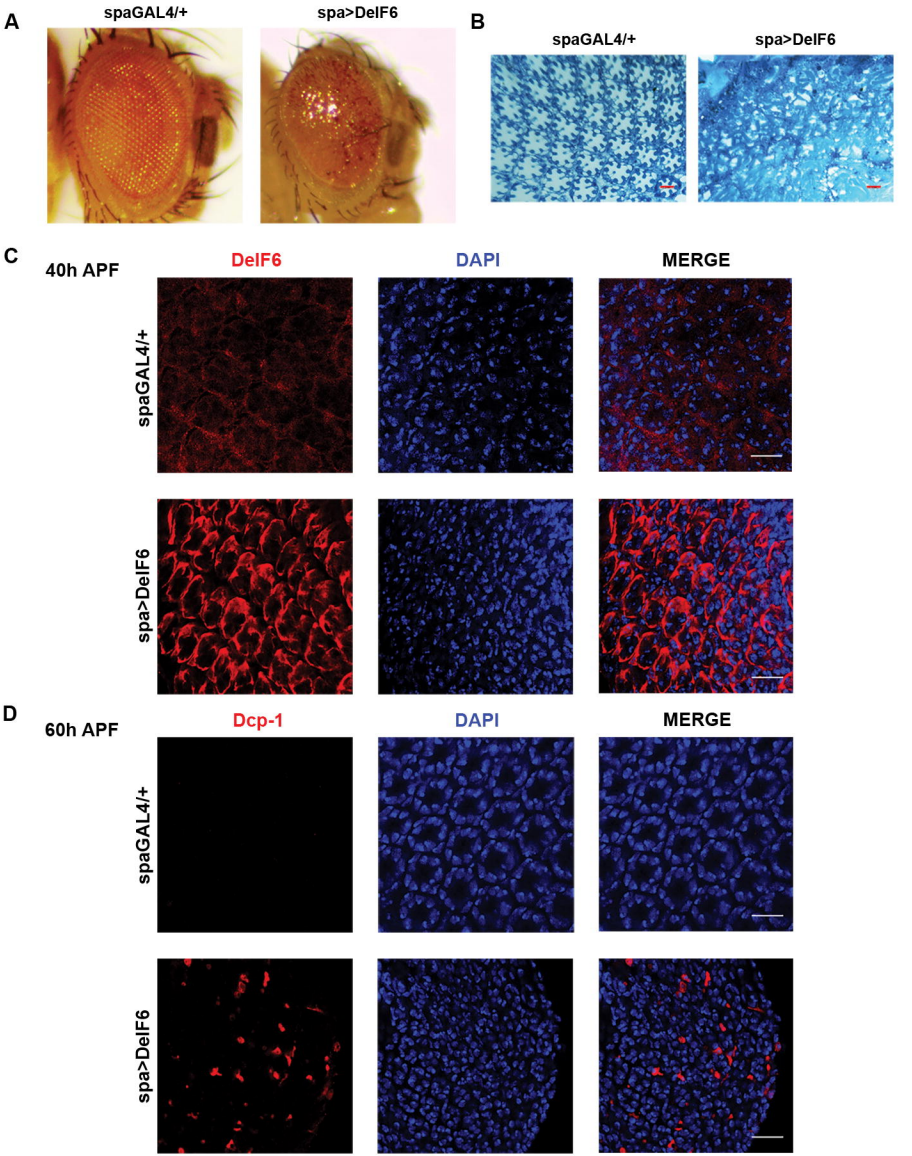
A
spaGAL4/+
spa>DelF6
B
spaGAL4/+
spa>DelF6
C
40h APF
DelF6
DAPI
MERGE
spaGAL4/+
spa>DelF6
D
60h APF
Dcp-1
DAPI
MERGE
spaGAL4/+
spa>DelF6

A

MSGAL4/+
MS>DelF6

B

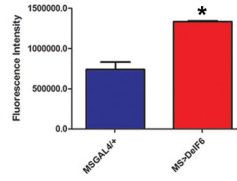
SUnSET Assay
1500000.0
1000000.0
500000.0
0.0
Fluorescence Intensity
*
MSGAL4/+
MS>DelF6

C

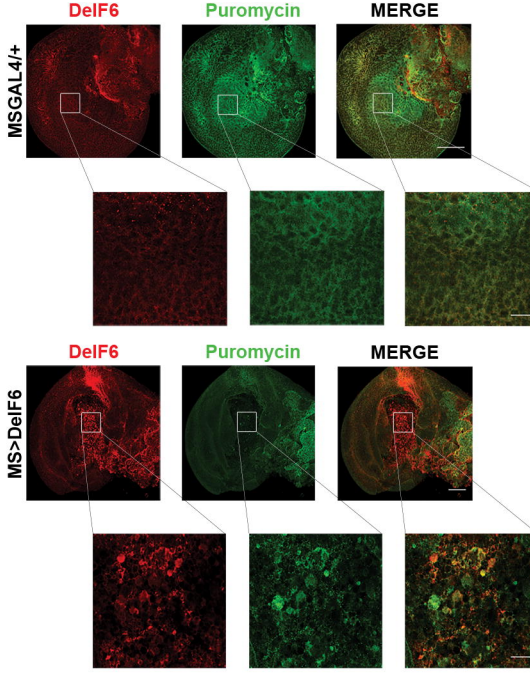
DelF6
Puromycin
MERGE
MSGAL4/+
DelF6
Puromycin
MERGE
MS>DelF6

D

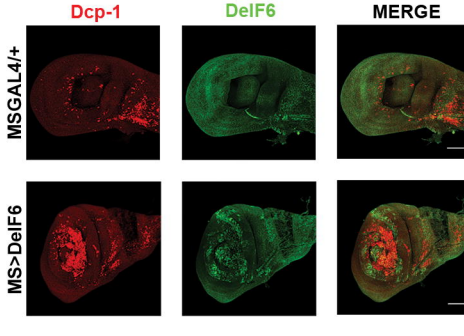
Dcp-1
DelF6
MERGE
MSGAL4/+
MS>DelF6

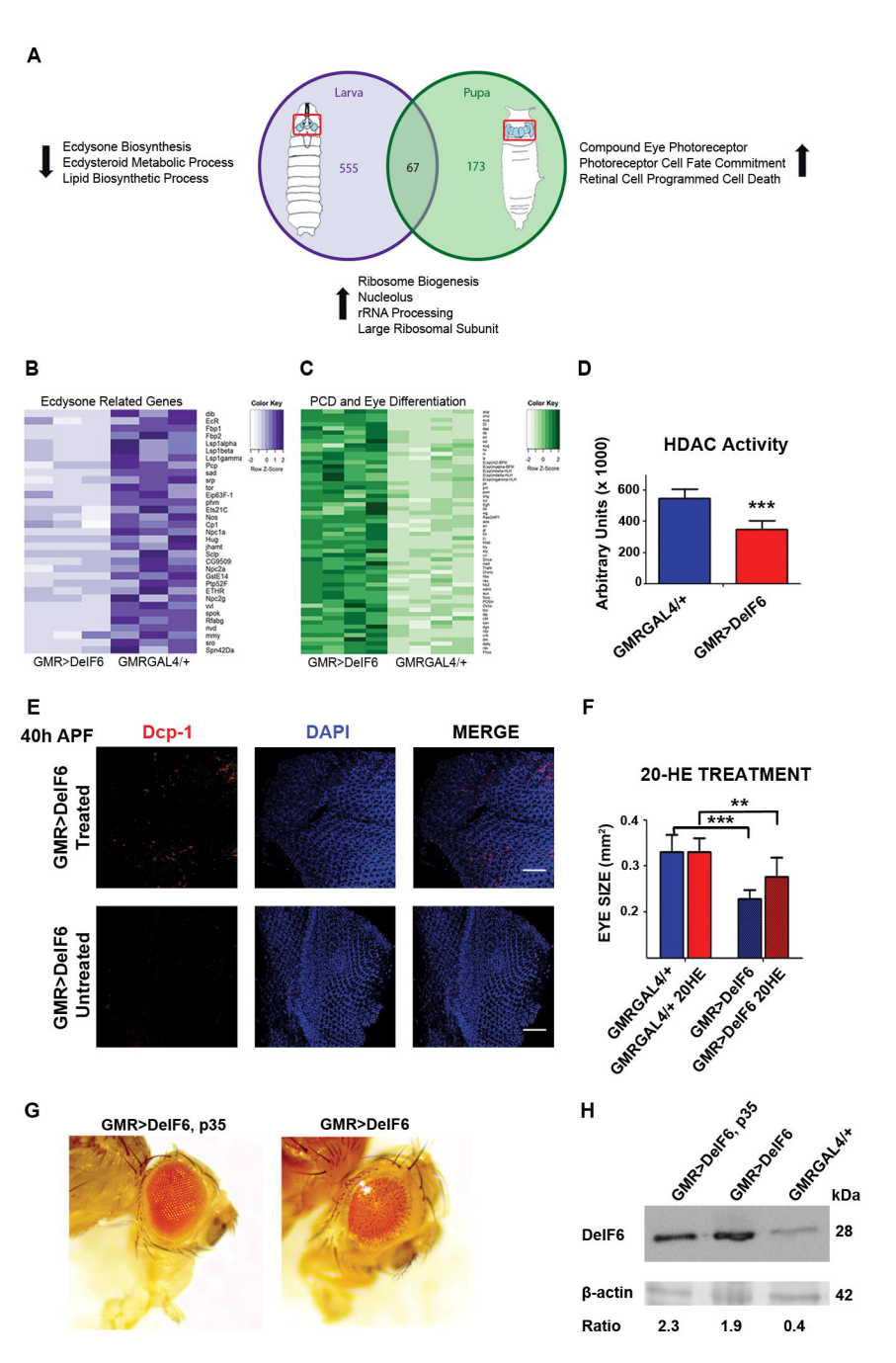
A
Larva
Pupa
555
67
173
Ecdysone Biosynthesis
Ecdysteroid Metabolic Process
Lipid Biosynthetic Process
Compound Eye Photoreceptor
Photoreceptor Cell Fate Commitment
Retinal Cell Programmed Cell Death
Ribosome Biogenesis
Nucleolus
rRNA Processing
Large Ribosomal Subunit
B
Ecdysone Related Genes
Color Key
Row Z-Score
GMR>DelF6
GMRGAL4/+
C
PCD and Eye Differentiation
Color Key
Row Z-Score
GMR>DelF6
GMRGAL4/+
D
HDAC Activity
Arbitrary Units (x 1000)
600
400
200
0
***
GMRGAL4/+
GMR>DelF6
E
40h APF
Dcp-1
DAPI
MERGE
GMR>DelF6 Treated
GMR>DelF6 Untreated
F
20-HE TREATMENT
EYE SIZE (mm²)
0.4
0.3
0.2
**
***
GMRGAL4/+
GMRGAL4/+ 20HE
GMR>DelF6
GMR>DelF6 20HE
G
GMR>DelF6, p35
GMR>DelF6
H
GMR>DelF6, p35
GMR>DelF6
GMRGAL4/+
kDa
DelF6
28
β-actin
42
Ratio
2.3
1.9
0.4

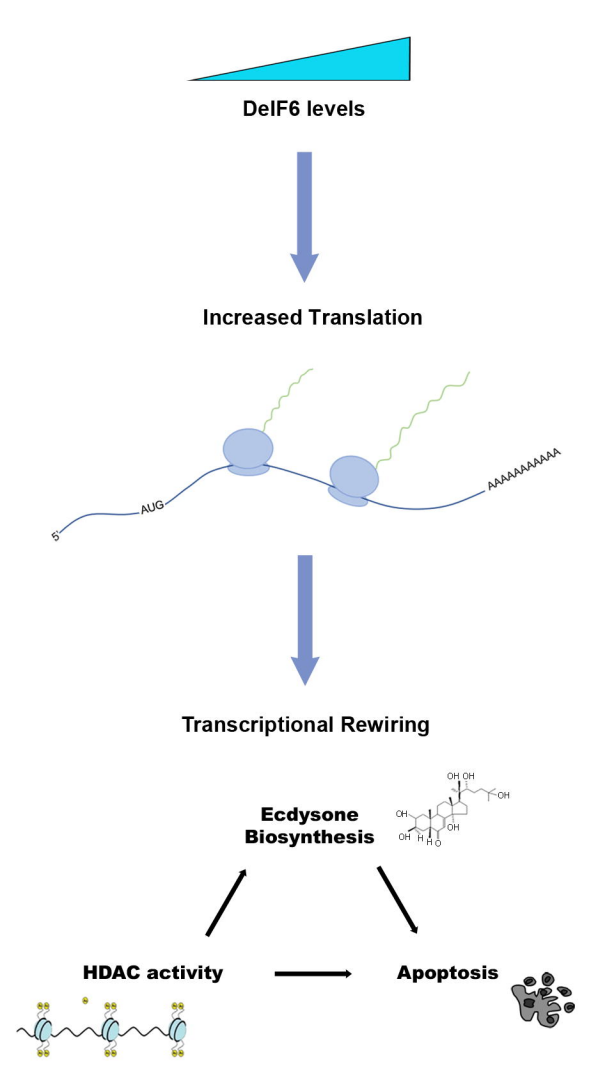
DelF6 levels
Increased Translation
5'
AUG
AAAAAAAAAA
Transcriptional Rewiring
Ecdysone Biosynthesis
OH OH
OH
OH
OH
OH H H O
HDAC activity
Apoptosis

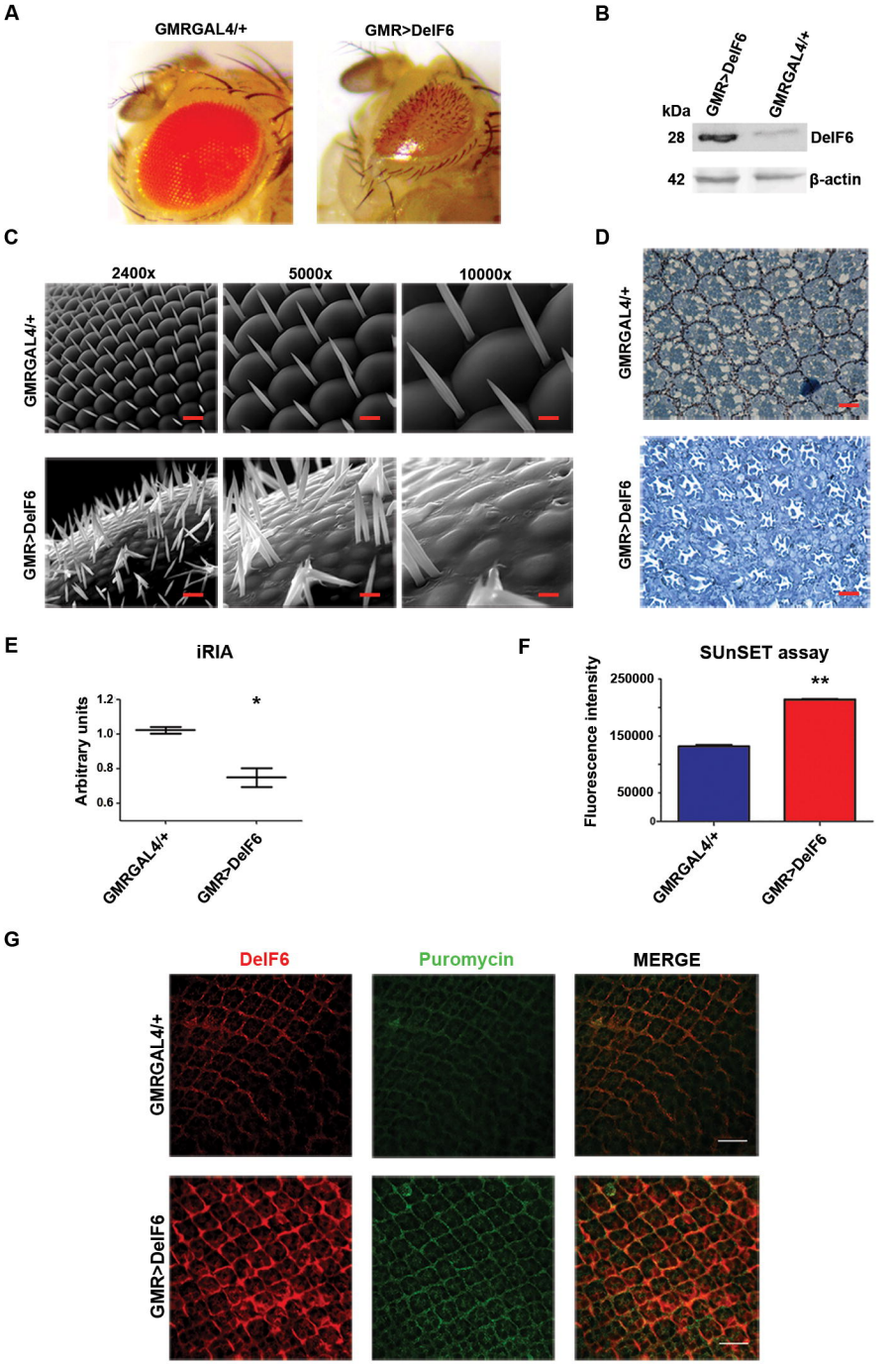
A
GMRGAL4/+
GMR>DelF6
B
GMR>DelF6
GMRGAL4/+
kDa
28
DelF6
42
β-actin
C
2400x
5000x
10000x
GMRGAL4/+
GMR>DelF6
D
GMRGAL4/+
GMR>DelF6
E
iRIA
Arbitrary units
1.2
1.0
0.8
0.6
*
GMRGAL4/+
GMR>DelF6
F
SUnSET assay
Fluorescence intensity
250000
150000
50000
0
**
GMRGAL4/+
GMR>DelF6
G
DelF6
Puromycin
MERGE
GMRGAL4/+
GMR>DelF6

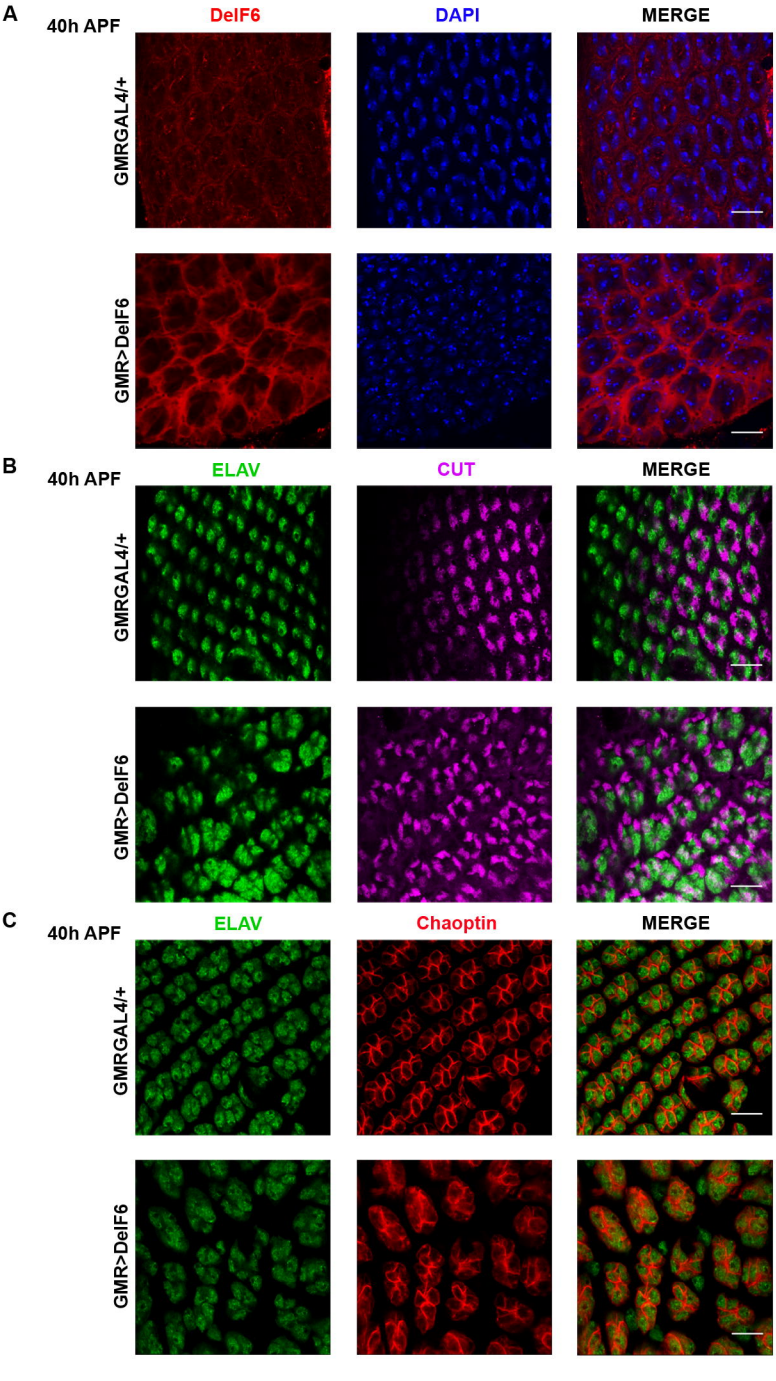
A
40h APF
DelF6
DAPI
MERGE
GMRGAL4/+
GMR>DelF6
B
40h APF
ELAV
CUT
MERGE
GMRGAL4/+
GMR>DelF6
C
40h APF
ELAV
Chaoptin
MERGE
GMRGAL4/+
GMR>DelF6

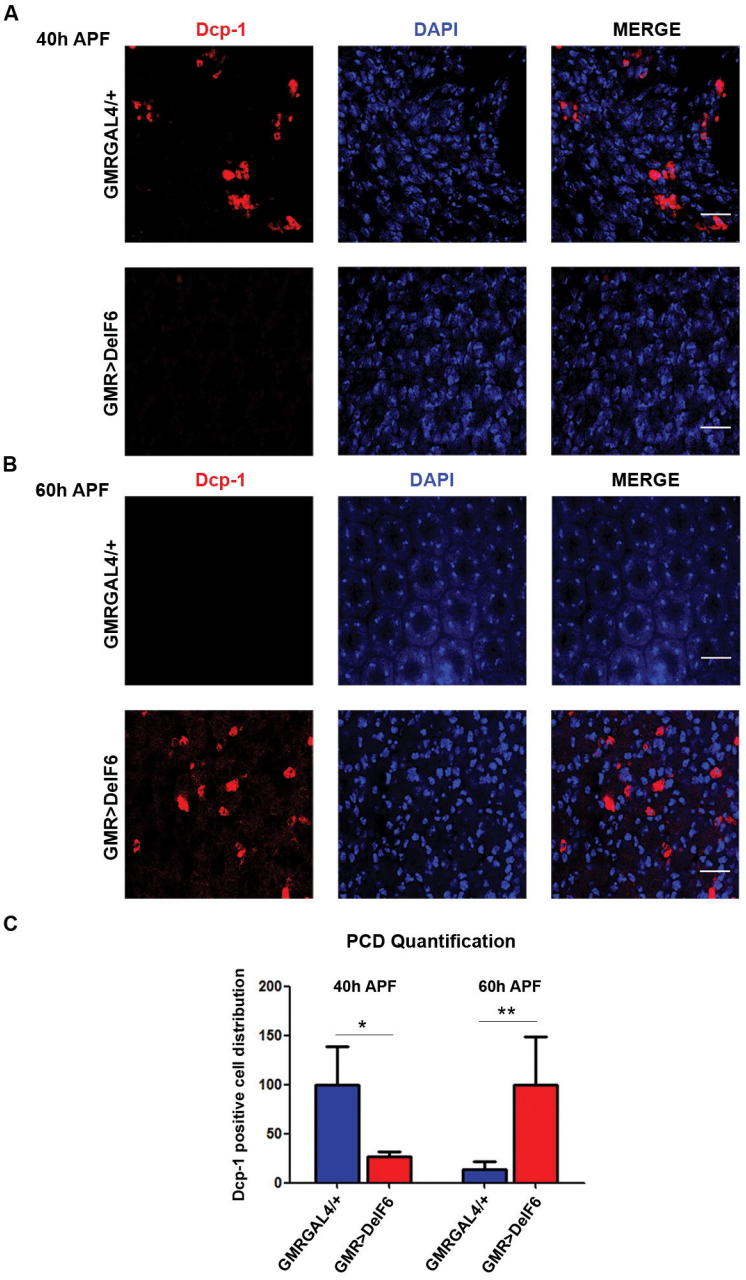
A
40h APF
Dcp-1
DAPI
MERGE
GMRGAL4/+
GMR>DelF6
B
60h APF
Dcp-1
DAPI
MERGE
GMRGAL4/+
GMR>DelF6
C
PCD Quantification
Dcp-1 positive cell distribution
200
150
100
50
0
40h APF
60h APF
*
**
GMRGAL4/+
GMR>DelF6
GMRGAL4/+
GMR>DelF6